A Global Assessment of the Mosaic Approach to Modeling Land Surface Heterogeneity

Andrea Molod *
Department of Earth and Planetary Sciences
The Johns Hopkins University, Baltimore, MD 20812

and

Haydee Salmun
Department of Geography and Environmental Engineering
The Johns Hopkins University, Baltimore, MD 20812

July 11, 2001

* Also: Data Assimilation Office, Goddard Space Flight Center, Greenbelt, MD 20771
Corresponding author address: molod@rua.eps.jhu.edu

Abstract

Modeling the impact of small scale land surface heterogeneities on scales resolved by General Circulation Models (GCMs) has long been a challenging problem. We present here a global offline comparison between two approaches to account for the heterogeneities. These approaches are mosaic, which computes separate energy budgets for each surface type within a grid box, and dominant, which assumes that a grid box can be completely described by the dominant vegetation. The experiments are all conducted using the turbulence parameterization of the Goddard Earth Observing System (GEOS) GCM, coupled to the Koster-Suarez Land Surface Model. The results show a large impact in the high and mid-latitude northern hemisphere climates. At high latitudes, the warming of the surface after the spring snow melt is more rapid for dominant. At mid-latitudes, where the surface is potentially under moisture stress, the mosaic approach results in a drier, warmer climate. This impact is determined to a large extent by the influence of bare soil areas on the grid scale climate. The impact of the choice of approach is less important over more homogeneous terrains, such as deserts, as can be expected in the offline framework. These results support the need for a mosaic-type approach to properly model the coupling at the land surface interface.

1 Introduction

The energy and material exchanges that occur at the land surface make it a critical component of the earth's climate system. These exchanges act to partition the net radiation into surface heating, deep soil heating, sensible and latent heat fluxes, to redistribute precipitation into evaporation, soil storage, groundwater recharge and runoff, and to regulate biogeochemical cycles such as photosynthesis, transpiration, the nitrogen cycle, and carbon uptake. The surface fluxes are known to significantly influence rainfall, temperature and circulation, [*Milly and Dunne*, 1994; *Polcher*, 1995] from daily to inter-glacial scales. A recent study shows that the energy exchanges that occur at the land surface are instrumental in effecting the interactions between different modes of climate variability [*Wu et al.*, 1999]. Because so much of the climate signal resides in the predominant modes of variability other than the mean, capturing these modes and their interactions in global models is crucial to climate prediction [*Leetma and Higgins*, 1999].

The heterogeneities in the land surface on scales smaller than the typical grid scale of current General Circulation Models (GCMs) have made it difficult to simulate the mean climate. The difficulty resides in properly capturing the impact of the subgrid scale variability on the grid scale. Almost all the Soil-Vegetation-Atmosphere-Transfer (SVAT) models that are coupled to state of the art regional and global climate models employ some technique to attempt to account for the subgrid-scale heterogeneities. Comparisons between these different schemes have served to demonstrate the strengths and weaknesses of the schemes, and also to aid in the understanding of the influence of small scale land surface heterogeneity on the atmospheric boundary layer and climate.

The earliest of the SVAT formulations for GCMs assumed that the land surface in a GCM grid square can be adequately described by the 'dominant' soil and vegetation characteristics from climatology [*Dickinson et al.*, 1986]. A single set of parameters is specified in the dominant technique which realistically describes the most frequently occuring vegetation and soil type in any GCM grid box. An advantage of this technique (unlike the 'composite' technique described below) is that it specifies only combinations of vegetation characteristics that are found in nature. The dominant technique cannot, however, account in any way for the existence of other vegetation and soil types that may exist over significant areas of the grid box.

The majority of the GCMs that are participating in the Atmospheric Model Intercomparison Project (AMIP) II [*Gates*, 1995] account for the subgrid-scale variability by specifying soil and vegetation parameters that represent a homogeneous 'composite' vegetated surface and its underlying soil for each GCM grid square. Among these are the GCMs used at the ECMWF [*Viterbo and Beljaars*, 1995], NCAR [*Gates*, 1995], NCEP [*Pan and Mahrt*, 1987], the Center for Ocean-Land Atmosphere Studies [*Xue et al.*, 1991], the Canadian Climate Centre [*Verseghy et al.*, 1993], and Météo-France [*Mahfouf et al.*, 1995]. There are various different techniques for calculating the appropriate grid-scale vegetation and soil characteristics (e.g., *Henderson-Sellers and Pitman* [1992]), but in general the parameters are aggregated linearly, except the roughness length. The aggregated roughness length is computed so as to approximate a linear aggregation of the turbulent momentum flux. A technique that can be viewed as a form of composite is the mixture technique [*Sellers et al.*, 1986], in which up to two vegetation types can occur simultaneously, that is, one atop the other, in a grid box. Mixture is similar to composite in that in both techniques it is assumed that there is horizontally uniform coverage of a combined vegetation type in a grid box.

A few of the AMIP II GCMs and some others account for the subgrid-scale heterogeneity using a scheme referred to as the 'mosaic' approach. Separate heat and moisture balance equations are solved for each vegetation type contained within a GCM grid square and the resulting heat and moisture fluxes which describe the coupling to the atmospheric boundary layer are aggregated linearly. These are the GCMs used at the Goddard Institute for Space Studies [*Rosenzweig and Abramopoulos*, 1997], Laboratoire Météorologie Dynamique [*Ducoudre et al.*, 1993], the Australian Bureau of Meteorology Research Centre [*Desborough and Pitman*, 1998], and the NASA/Goddard Seasonal to Interannual Prediction Project [*Koster and Suarez*, 1992a]. The turbulent diffusion in the boundary layer and above is then computed based on the grid-averaged surface flux of heat and moisture. The statistical-dynamical representations of the subgrid heterogeneity, in which probability distributions for vegetation parameters in a grid box are specified, may be viewed as another type of mosaic representation (e.g., *Entekhabi and Eagleson* [1989] and *Avissar* [1991]).

Many intercomparisons exist between the commonly used techniques to account for subgrid scale variability. Comparisons between dominant and composite, or between different input parameter values in the composite strategy, have been made both on a global and a local scale. *Arain et al.* [1999] compared the composite and the dominant techniques in ten year simulations with NCAR's Community Climate Model version 3, and found that the composite technique resulted in potentially large differences in simulated surface fluxes and temperature, and improved the simulations over the Sahara desert and the Himalayan mountains. The sensitivity of surface fluxes to the choice of input parameters in a composite technique was performed by *Xue et al.* [1991]. They showed typical differences in monthly mean latent heat flux of 9 W/m^2, and seasonal differences of 2 W/m^2 when the input leaf area index and albedo were changed based on modern estimates of these parameters.

The comparisons between mosaic and composite are mostly local in nature. A direct comparison of the mosaic and composite methodologies during July over the east-central USA was performed by *Klink* [1995], and demonstrates an improved simulation of the local climate using the mosaic approach. A comparison of mosaic and mixture for a terrain type which is homogeneously covered by two vegetation types (savannah, where mixture is an accurate representation) was performed by *Koster and Suarez* [1992b], who showed that the resulting fluxes using the mosaic approach are quite close to the mixture results. Studies by *Cooper et al.* [1997], *van den Hurk and Beljaars* [1996], *Arola and Lettenmaier* [1996] and *Polcher et al.* [1996] all reported significant differences between mosaic and composite during the spring and summer at several different northern hemisphere locations. These studies find that the mosaic representation reduces the latent heat fluxes (and increases the sensible heat), and offers the more accurate estimates of surface fluxes. *Mölders et al.* [1996] compared the mosaic technique for a central European location in springtime to a fine mesh model and found that the mosaic technique might tend to underestimate the latent heat flux.

The local nature of the comparisons between mosaic and composite makes it difficult to generalize the results to different geographic regions, climate regimes or different seasons. The present work addresses this issue by focusing on a global comparison of the dominant and mosaic techniques in order to evaluate the impact of modeling technique on the global climate. Differences will be assessed for a varied set of climate regimes and vegetation types throughout the entire annual cycle. This study was conducted in an offline modeling framework, which allows the analysis of direct differences, without the additional variability of potential climate feedbacks. The global offline experiments constitute a baseline for fully prognostic studies. The experimental design is described in the following section, along with a brief description of the model used. Results are presented in section 3. Conclusions from this study are presented in the summary of the final section, along with some comparisons with previous studies.

2 Offline Modeling Framework

The offline experimental framework is the Offline Land GEOS Assimilation (OLGA), developed by *Houser et al.* [1997]. OLGA uses the Goddard Earth Observing System-Version 1 Data Assimilation System (GEOS-1 DAS) reanalysis [*Schubert et al.*, 1993] near surface fields to drive a coupled land surface exchange system. The system consists of the *Koster and Suarez* [1992a, c] land surface model (hereafter referred to as KS LSM) coupled to the GEOS-Terra turbulence and surface layer parameterization [*Helfand and Labraga*, 1988; *Helfand and Schubert*, 1995] in the manner described in *Molod* [1999]. This coupled system uses a mosaic type approach to model the impact of the subgrid scale variability with a technique that is called ‘extended mosaic’. ‘Extended mosaic’ differs from a standard implementation of a ‘mosaic’ scheme in that it extends the independent calculations of the turbulent fluxes over each ‘tile’ to the top of the model's atmosphere. For the offline experiments of this study, where the atmospheric state is supplied at every time step (as described below), the differences between the standard ’mosaic’ and ‘extended mosaic’ techniques are near zero. We will therefore refer to the ‘extended mosaic’ experiments as ‘Mosaic’ (M). OLGA was also used to perform an experiment using the ‘dominant’ technique (D).

A schematic of the OLGA experimental framework is shown in figure 1. An initial state for the surface and soil is provided from a five-year GCM simulation to ensure the proper balance between the surface and the deep soil state. Atmospheric conditions, including temperature, humidity and winds from the GEOS-DAS (data flow indicated by light arrows in the figure) are used in the GEOS-Terra turbulence scheme to compute turbulent fluxes at the surface and throughout the boundary layer. The sequence of processes in OLGA is indicated by the heavy arrows in the figure. The turbulent fluxes, along with the net radiation, precipitation and Photosynthetically Active Radiation (PAR) from the DAS, are then used by the KS-

LSM to compute a new surface and soil state. The turbulent fluxes are then updated based on this new surface and soil state to guarantee that the computations conserve energy and moisture. The time integration proceeds with the new state, as indicated by the heavy arrow, and with the next input of atmospheric fields from the DAS.

The surface and soil state consists of the surface skin temperature, T_c, (which we call canopy temperature, as is done in *Koster and Suarez* [1992a]), the deep soil temperature, T_d, the near-surface air specific humidity, q_a, (which we call canopy humidity), the snow amount, the canopy interception reservoir amount, C, and three levels of soil moisture, W_{shal}, W_{root} and W_{deep} respectively. The temperature budget is solved in each of two layers, the upper one represents the vegetation canopy and the soil surface and the lower one represents the deep soil temperature. The moisture budget is solved in each of three layers. The thickness of the top layer ranges from 0.9 to 2 cm and represents surface shallow processes, the second layer represents the root zone and ranges from 0.9 cm to 1.4 m in thickness and the third layer, referred to as the recharge layer, ranges from 0.3 to 2 m in depth. Above the land surface, OLGA calculates turbulent fluxes of heat and moisture for three atmospheric levels, which approximatelly constitute the planetary boundary layer. A full boundary layer calculation is performed because turbulence is modeled as a diffusion process with a zero flux boundary condition at the top of the planetary boundary layer.

The OLGA time integration is performed using a time step of five minutes, which is commensurate with the shortest time scales of physical processes at the land surface, and ensures numerical stability of the calculations. Since the fields from the DAS are available at six hour intervals, OLGA performs a linear interpolation to obtain forcing data at five-minute intervals. This interpolation scheme has the potential to substantially underestimate the precipitation intensity and thus impact the amounts of runoff and infiltration. These errors may impact the D and M experiments differently. Although more sophisticated algorithms to interpolate precipitation fields have been used (e.g., the GCIP Land Data Assimilation System Project [*Mitchell et al.*, 1999]), the accurate partition of precipitation into infiltration and runoff is not a paramount goal in this study and the linear interpolation is adequate.

The radiative forcing from the DAS in OLGA is the net shortwave and net longwave radiation. Specifying the net radiation implies that two important feedback mechanisms are absent. The albedo is specified implicitly in the net shortwave, based on the snow cover in the DAS, and the snow-albedo feedback, which serves to cool a snow-covered surface, is removed in OLGA. The outgoing longwave is also specified, based on the surface temperature in the DAS, and the ability of a warming surface to be cooled by emitting radiation is also absent. There is, however, a small correction in the outgoing longwave radiation of the order of $1-2\%$ to account for the instantaneous changes in surface temperature. This does not represent a significant longwave radiation feedback. Other offline simulations specify the incoming solar radiation and the downwelling longwave radiation, allowing the albedo feedback due to the presence of snow, and the longwave feedback to respond to changes in surface temperature (The Global Soil Wetness Project (GSWP), *Dirmeyer et al.* [1999], for example). This approach provides a more accurate simulation, as was needed for GSWP to obtain accurate estimates of soil moisture. Specifying the net radiation at the surface, however, as is done in OLGA, ensures that the net energy available to the surface is identical in both the D and M experiments. This, in turn, allows us to assume that the causes for the differences between experiments are due to the handling of the surface heterogeneity.

A crucial aspect of the present experiments is that an identical model is used in both offline experiments. The 'dominant' and 'mosaic' experiments differ only in their specification of the number of 'tiles' in any grid box. The differences between experiments therefore are due to this aspect of handling the land surface heterogeneity alone, and not due to any differences between models. The intercomparisons between mosaic and composite in other studies, such as those using the PILPS experiments (e.g., *Chen et al.* [1997]), include differences due to model formulation as well as differences in the philosophy of how to handle the heterogeneities.

The sub-grid scale variability of the surface is modeled in the KS LSM by viewing each GCM grid cell as a mosaic of independent vegetation stands. The vegetation stands, or 'tiles', do not interact at all in the OLGA experiments described here. The KS LSM approach to handling sub-grid scale heterogeneities is presented schematically in the 'mosaic' panel of figure 2, where a hypothetical GCM grid square containing the 'tiles' that describe the mix of surface scene types is shown. The figure also depicts the 'dominant' and 'composite' approaches. In the mosaic approach, all of the bare soil portions of the grid box are treated as though they are juxtaposed, as are all of the deciduous trees, evergreen trees, and shrubs. Each of these types is assigned a fraction of areal coverage, which is used to compute grid box averaged fluxes by aggregating linearly. The surface types and the percent of the grid cell occupied by any surface type were derived from the surface classification of *Defries and Townshend* [1994], and information about the location of permanent ice was obtained from the classifications of *Dorman and Sellers* [1989]. The geographical distribution of surface designations at $1°$x$1°$ resolution is shown in figure 3. Each tile in a grid box, with its own canopy temperature, is assumed to underly an atmosphere with the same grid mean air temperature. The individual tile values of the change in canopy temperature and humidity computed in the KS LSM are used to provide values of the surface fluxes of heat and moisture, and these surface fluxes are aggregated linearly to provide a single grid-averaged value of the flux across the bottom boundary.

We elected to conduct our extended mosaic (M) and dominant (D) experiments using the GEOS-1 DAS reanalysis from 1991 to drive OLGA, because the low Southern Oscillation Index during that year allows us to consider 1991 an average climatological period. It should be noted that the GEOS-1 DAS atmospheric forcing contains some serious biases, as documented by *Schubert et al.* [1995] and *Molod et al.* [1996]. The most egregious of these is the severe wintertime cold bias near the surface, which affects the springtime snow melt.

3 Results

We present our results in the form of time series of regional averages. Fifteen regions were identified, representing separate seasonal and climatic regimes, each approximately 20^o of longitude by 12^o in latitude in area. They are listed in Table 1, and indicated by the boxes drawn in figure 4. The distribution of land surface types and their fractional contribution to the grid average for each region is seen in the vegetation map, figure 3. Each colored area in the figure refers to a particular distribution of tiles, and although each region is not covered by a unique distribution, a predominant distribution for each region is discernable. We examine the grid-averaged differences between the D and M experiments as well as the behavior of each of the different vegetation types or 'tiles' in several of the fifteen regions. The grid-averaged differences provide insight into the implications on the regional and global climate scale of the handling of the surface heterogeneity, while the tile space behavior allows us to evaluate the contributions of the different surface types to the differences seen at the grid scale.

In order to get a sense for the geographical locations where the technique of modeling the subgrid scale heterogeneity might be expected to produce differences in the local climate, we have defined a 'Variability Index' (VI) to describe the area of a grid square occupied by some vegetation type other than the predominant type for that grid. We define:

$$VI \;=\; (1 - F_d)^2 \;,$$

where F_d is the tile fraction of the predominant land surface type. The variability index is plotted in figure 4, and regional averaged values for VI are listed in Table 1. The figure shows that VI is largest over much of the northern hemisphere extra-tropics. The smallest values of variability are over desert regions, glaciers, and the tropical rain forests.

Results from the fifteen different regions fell into general groups. The first general group, which we designate Northern hemisphere High Latitude climates (NHL), are Alaska, Siberia, Russia, Newfoundland and Boreal Forest. These regions roughly correspond to the 'microthermal moist' climate as defined in the Koeppen system [*Koeppe and DeLong*, 1958]. This group exhibits D-M differences that are largest in the late spring and early summer, and determined by the behavior of the energy budget during the spring snowmelt, as will be elucidated below. The next general group to be presented in detail is made up of the Northern hemisphere mid-latitude regions, which we designate NML (China, Central Plains, Eurasia and Southeast U.S.). These regions roughly correspond to the 'mesothermal moist' climate of the Koeppen system, and all show patterns of D-M differences that are largest in late summer, connected to the budget of summertime canopy humidity. Desert climates, such as Sahara, with variability index less than 5, exhibited little difference between M and D, due to the homogeneous character of the surface (low VI). Southern Africa exhibits some behavior in common with the NML regions, and D-M differences were observed for the Central South America and Southern South America as well. A Student's t-test for the mean differences and an F-test for the variance of the differences were performed, and both show statistical significance of the differences with 98% confidence in all regions except Sahara, Amazon and Australia.

3.1 Northern High Latitude Regions

The largest D-M differences in grid-averaged canopy temperatures were seen in the northern hemisphere high latitude (NHL) regions. Figure 5 shows the time series of canopy and deep soil temperatures (5a) and shallow and root zone soil moistures (5c) for the D and M experiments, as well as their D-M differences (5b and 5d) for the Russia region, which is typical of NHL. The annual cycle of Russian canopy and deep soil temperatures, figure 5a, shows the rapid warming after the spring snow melt. The M results (dashed lines) indicate an average February to April warming rate of $12.0K$ per month, which is somewhat slower than the D results (solid lines), in which we obtain an average warming rate of $12.5K$ per month. The deep soil temperature annual cycle lags behind the canopy temperature, as expected, by almost two months, and is approximately $6K$ smaller in amplitude. The shallow soil moisture, 5c, peaks during the winter because of the presence of snow, and is minimum, although still moist, in summertime. The root zone soil moisture, on the other hand, is maximum in summertime, related to the precipitation and infiltration of the water. Figure 5b and 5d show the differences of temperatures and soil moistures respectively. The peak differences in canopy temperature are in the spring, when the faster warming rate in the D experiment results in a canopy which is approximately $1.5K$ warmer than the canopy in the M experiment, and in the fall, when the canopy in the D experiment is almost $1K$ colder than in M. These differences are of the same order as differences between model experiments reported in the PILPS intercomparison (e.g., *Chen et al.* [1997]). Differences in deep soil temperature and surface soil moisture peak in mid-summer, and the root zone soil moisture differences exhibit little annual cycle.

All of the NHL regions exhibited this behavior in the period immediately following the start of the spring snow melt. Figure 6 shows that the peak of the D-M differences in T_c over Alaska (top curve) occurs between March and April, and occurs later in the year as we move down through the curves (in sequence, Newfoundland, Boreal Forest, Russia, Siberia) to colder regimes, with the latest peak in June (bottom curve). The key feature of the results from the NHL regions is the more gradual warming rate in the mosaic approach.

In order to gain some understanding of the physical mechanisms that may explain the observed differences between our experiments, we examine the surface energy balance equation

$$C_h \frac{\delta T_c}{\delta t} \;=\; R - \lambda E - H - G - S_m \; .$$

In this expression T_c is the canopy temperature, C_h is the canopy heat capacity, R is the net radiation at the surface, λE is the latent heat flux, H is the sensible heat flux, G is the ground heat storage, and S_m is the energy used to melt the snow. We recall that in the OLGA framework the net radiation at the grid scale is specified, so any differences in the net surface heating between D and M must be due to differences in turbulent heat fluxes, ground storage, or snowmelt. These differences for the Russia region are shown in figure 7a, where 30 day running averages accentuate the seasonal trends. The differences in latent and sensible heat fluxes range between 5 and 10 W/m^2, which is again comparable to the differences between models reported in PILPS [*Chen et al.*, 1997]. The sign convention used is such that a positive contribution to the net canopy heating term (warming) is represented by the positive values of the curves in the figure. Throughout most of the year, therefore, we see that the D-M differences in sensible heat flux represents a warming in D relative to M, while in the summertime the D-M differences in latent heat flux contribute to a cooling. This is in qualitative agreement with the study of *Cooper et al.* [1997] over the Canadian boreal forest in summertime, who found that the latent heat flux was increased substantially by using a composite soil moisture as compared with either a mosaic approach or *in situ* observations.

Further inspection of the figure 7a shows the near exact balance between the turbulent flux (LE+H, the blue curve) and the ground storage terms (green curve) throughout the year. A closer look at this balance using daily means during the winter and springtime reveals that the residual of these two large terms, shown in figure 7b, is responsible for the differences in heating rates in the winter and spring, and therefore for the differences in canopy temperatures. The red curve in figure 7b is the heating rate in energy units (W/m^2), and the black curve whose temporal variations and magnitude closely follow the heating is the residual of the turbulent fluxes and ground storage. The ground storage term, which may be viewed as a heat conduction between the surface and the deep soil, is formulated in the KS-LSM using a force- restore scheme, and is neccesarily a response to the net radiative and turbulent heat flux at the surface. The ground storage, therefore, cannot be the physical mechanism driving the D-M differences in canopy temperature, and we conclude that it is the differences in turbulent fluxes that are causing the canopy in the D experiment to be warmer than in the M experiment. Since the wintertime turbulent fluxes are downward, the negative D-M difference of the turbulent fluxes indicates that the M experiment results in a suppressed downward turbulent flux of energy during the winter and early spring. The larger downward turbulent heat flux in D is the cause for the warmer canopy temperatures in that experiment. The sensible heat flux is the dominant turbulent flux in the wintertime, and consequently dominates the D-M differences. Insight into the differences in the sensible heat flux between D and M can be gained by comparing tile space results to get an indication of the contributions of the various vegetation types to the grid average.

We performed regional tile space averages over a contiguous subregion of Russia (60N to 64N and 90E to 100E) where the vegetation cover in each grid box consists of 38% deciduous trees, 37% needleleaf trees and 25% bare soil. This distribution of vegetation is typical of NHL. Figure 8 shows the daily time series of the canopy temperature (8a) and sensible heat (8b) differences between each of the off-dominant tiles and the dominant deciduous trees tile in the M experiment. We can see from the figures that the largest differences occur over the bare soil tile, and it is these differences that determine the grid-averaged D-M behavior shown in figure 7. Figure 8b shows that the downward sensible heat flux, which we determined was the key factor in the surface energy budget, is smaller over the bare soil tile than over either one of the vegetated tiles. Another contiguous subregion of Russia was examined where the dominant vegetation type is needleleaf trees and the results (not shown here) are essentially the same, supporting the conclusion that the bare soil tile behaves differently from either vegetated tile. Further support for the importance of the bare soil tile in determining the climate response to a mosaic-type modeling approach comes from examination of results from two typical grid points in NHL. Figure 9 contrasts the bare soil minus dominant tile canopy temperature difference with the tree-covered tile minus dominant tile difference for grid boxes with two different dominant surface types. The solid lines in the figure, which are the bare soil minus dominant differences, are clearly almost an order of magnitude larger than the differences between the tree covered tiles, and this is true when either tree tile is dominant in the grid.

We understand this difference in the behavior of the sensible heat flux over the bare soil tile in the context of the fractional area of snow coverage for each of the tiles. Insofar as the snow acts to insulate the surface from the lower atmosphere, a higher fractional snow coverage will act to suppress the surface-atmosphere exchange. Figure 10 shows a subregion averaged time series of the fractional area of snow cover for each of the tiles present. It is clear that the bare soil tile has the greater extent of snow cover and so would have the lower temperature and the lowest sensible heat fluxes. A two-year offline study over western Montana by *Arola and Lettenmaier* [1996] also found that the mosaic formulation resulted in a snow cover that persisted further into the spring because of the ability to capture the behavior over the high elevation regions. They found that associated with the increased presence of snow in mosaic relative to composite there is a decreased latent heat flux, with the biggest differences occurring when all snow had melted in their composite experiment but snow persisted in mosaic. Our results, therefore, further support that the differences in behavior between bare and vegetated areas during the snow cover and snow melt seasons need to be considered in the proper modeling of the regional climate.

3.2 Northern Middle Latitude Regions

Typical Northern Mid-Latitude (NML) region behavior is described in figure 11, where the temperatures, canopy humidities and latent heat fluxes for the D and M experiments in the Central Plains region are shown. The annual cycle of the canopy and deep soil temperatures, figure 11a, are quite similar to those from NHL, except for the expected shift towards warmer temperatures. The canopy and deep soil temperature D-M differences, seen in figure 11b, are smaller than they were in NHL, and indicate that the D experiment results in colder temperatures throughout the year, with peak difference in August. The amplitudes of the annual cycles of the temperature and its D-M difference are each approximately half the magnitude of the corresponding annual cycle in NHL, but the ratio of the amplitudes is comparable. This means that D-M canopy temperature differences in NML are of the same order as NHL when measured relative to the amplitude of the annual cycle. Figure 11c shows that the annual cycles of canopy humidity and latent heat flux are closely related, which reflects the fact that the magnitude of the canopy humidity is related to the latent heat flux. The same relationship is reflected in the D-M differences in these quantities, as shown in 11d.

To understand the D-M temperature differences in the NML region, we again look at the different terms in the surface energy balance equation. We see from figure 11b that the peak D-M canopy temperature differences occur in the summer, and we focus on the period immediately before. The terms of the surface energy budget are shown in figure 12a, where we again examine 30 day running means. As in figure 7a for the NHL region, a positive contribution to the net canopy heating term is represented by the positive values of the curves in the figure. In the summertime, therefore, we see that the D-M differences in latent heat flux (black curve) and in total turbulent flux (blue curve) represent a cooling in D relative to M, while the D-M differences in ground storage (green curve) and sensible heat flux (red curve) contribute to a warming. The increased latent heat flux in summertime in dominant relative to mosaic is in qualitative agreement with several studies conducted in several locations in NML types of climates. *Klink* [1995], in her study of conditions in Ohio (included in our Central Plains) in July, *van den Hurk and Beljaars* [1996], in a Mediterranean vineyard in June, and *Polcher et al.* [1996], in a one-year study over a semi-humid pasture in England and a semi-arid region in Spain, all found that a composite approach results in higher latent heat fluxes.

We see from figure 12a that the differences in total turbulent flux (LE+H, blue curve) during the summer are determined by the value of the latent heat flux. This is in contrast to the NHL region in winter and spring, where the D-M differences in total turbulent flux are determined by the sensible heat flux, and contribute to a warming at the surface in D relative to M. As in the NHL region, there is a close balance between the net turbulent flux and the net ground storage terms, which is to be expected because the ground storage is a response to the surface radiative and turbulent heating. The residual of these closely balanced terms is shown in the black curve of figure 12b, along with the D-M differences in total canopy temperature heating (in red). From these results we conclude that the canopy temperature heating differences are dictated by the latent heating.

The grid averaged D-M differences can be explained by considering the behavior of the different vegetation types in the NML regions. Figure 13 shows the differences in sensible and latent heat fluxes between the various off-dominant vegetation types and the dominant (grassland) vegetation type over the Central Plains region. Regional averaged characteristics for a particular tile type were obtained by area weighted averaging over the entire Central Plains region. The latent heat difference between the grassland tile and the bare soil tile, shown in 13a, follows the grid space D-M differences in latent heat seen in figure 11a. This is noteworthy given the relatively small areal fraction (approximately 25%) of the bare soil tile in the grid boxes. This difference in latent heat flux results in a grid averaged canopy that is loosing less heat and therefore is warmer in the M experiment. This effect is absent from the D experiment, of course, because only the dominant grassland is represented, but would also be absent from a 'composite' representation of surface heterogeneity over the Central Plains, since the area weighted characteristics will under-represent the actual influence of the bare soil tile. The dwarf tree tiles, and to a greater extent the deciduous tree tiles, are characterized by a larger evaporation than the grassland tile in the summertime, which is in contrast to the characteristic grid averaged behavior in the M experiment as compared to the D experiment. The dwarf tree and the deciduous tree tiles, therefore, cannot be characterizing the grid averaged behavior of the soil-canopy system, rather, the bare soil tile is determining the grid-averaged behavior of the latent heat differences. The determining influence of the bare soil tile is also seen in the sensible heat flux curve, figures 13b.

3.3 Other Regions

The results from the remaining regions showed little difference between D and M. The pattern of D-M differences in Central South America (not shown) are reminiscent of the NML regions. The maximum differences, however, occur in the southern winter rather than in the summer as in NML. The maximum differences in both cases occur in the season that has the annual minimum soil wetness, which results in a reduced latent heat flux from the bare soil. The results from Sahara show a small D-M difference in the values of T_c of approximately $0.3K$ throughout the year. The differences in other surface and soil variables are negligible, as is expected from the low value of the variability index. In the Amazon region the M canopy temperature is warmer by approximately $0.1K$ than in D. This represents 10%

of the amplitude of the annual cycle, and is commensurate with relative differences in other regions. In Australia the D-M canopy temperature differences are of the order of $0.5K$ throughout the year. As with Sahara and Amazon, differences in other surface and soil fields in Australia were negligible, and do not offer an explanation for the behavior of the temperatures. Southern Africa and Southern South America show D-M differences that are near zero.

4 Summary and Discussion

The impact on the simulated climate of the manner in which the heterogeneities in the land surface are modeled was examined over a wide range of climate regimes, and over regions with widely varying extents of surface variability. We presented differences between a dominant (D) technique and a mosaic (M) type approach, analysed the surface energy budget to illustrate the possible physical mechanisms underlying the differences, and evaluated the contributions of the different vegetation types. We found some correspondence between the extent of variability, as measured by VI, and the differences between modeling approaches, but the type of variability and the specific climate regime were also important factors in determining those differences.

The D-M canopy temperature differences were largest over the northern hemisphere high (NHL) and mid-latitude (NML) climates during the spring and summertime. The high latitude regions exhibit D-M differences that are determined by the behavior of the energy budget before and just after the spring snowmelt. The canopy in the M experiment warms up more slowly during the snowmelt than in the D experiment, because the high snow fraction over the bare soil area of the grid box inhibits the downward sensible heat flux and causes a colder surface. These findings are in qualitative agreement with existing studies in specific locations in NHL types of climates. The mid-latitude regions all show patterns of D-M differences that are connected to the summertime latent heat flux. The canopy in the M experiment is warmer than in D in the summer, resulting from a decreased latent heat flux due to the presence of the bare soil area in the grid. In both of these climate regimes, therefore, the largest D-M differences are dictated by the differences in how the contribution of the bare soil area to the grid average is modeled. An illustration of the critical role that the unvegetated surface plays in determining the climate reponse to the modeling approach is presented in figure 14, where the correspondence between global patterns of the off-dominant bare soil fraction and the largest monthly mean canopy temperature differences between D and M can be seen. The locations of the largest off-dominant bare soil presence are, in general, the locations of the largest D-M differences in canopy temperature.

In both NHL and NML regions, the bare soil tile dictated the grid-averaged behavior, although it only occupied 25% or less of the area. The influence of the bare soil, therefore, is larger than commensurate with its fractional coverage. This amplification of the influence would only be properly captured by a mosaic-type scheme. Moreover, in NML, the effect of the off-dominant vegetated tiles (deciduous trees and dwarf trees) on the grid-averaged canopy temperature is opposite in sign to the effect of the bare soil tile which still dictates the grid average. A composite approach which yields grid averaged characteristics closer to those of the trees would be unable to capture the grid-scale behavior. We argue therefore that modeling the surface heterogeneity as a mosaic of independant tiles and performing separate energy and moisture calculations is the scheme that can account properly for the behavior and influence of the bare soil areas in high and mid-latitude northern hemisphere climate regimes.

Results from the global offline OLGA framework experiments show a significant impact of the choice of modeling approach in the absence of climate feedbacks. The offline nature of the present study has allowed us to determine the importance of the unvegetated surface to the mean simulated climate. The global nature of the study, and the qualitative agreement with existing local comparisons, has allowed us to assess the suitability of the mosaic approach for predictive climate models. The work presented here is in qualitative agreement with several studies, for example, those of *Klink* [1995] and *Mölders et al.* [1996] which showed an improved simulation of climate using a mosaic-type approach when evaluated against an explicit sub-grid model, and of *van den Hurk and Beljaars* [1996] which showed a close correspondence between their mosaic experiment and *in situ* observations. We suggest that their conclusions about the adequacy of the mosaic approach may be extended to the entire mesothermal moist and microthermal moist climate regimes. This is important because it is the regional to global scale intercomparisons that are necessary to determine the modeling technique most appropriate for global climate models.

The OLGA results further serve as a guide for the next phase of the investigation, that of a fully-interactive GCM. This framework allows the fullest spectrum of interactions between elements of the soil-atmosphere system, and the contrast with the offline results will allow use to distinguish direct differences from climate feedbacks. Preliminary analysis of the GCM experiments shows that the differences between dominant and mosaic are amplified in some cases, as might be expected in a fully interactive experimental framework. In other cases, it appears that the feedbacks in the system give rise to a richer spectrum of responses to the differences between modeling techniques. Further work will consider a Data Assimilation System (DAS), and although it is a more externally constrained modeling system than a GCM, it provides the most realistic framework, because the evolution of the atmospheric state is constrained by observations. This hierarchy of frameworks, the offline, the GCM and the DAS, will be useful for testing other modeling techniques for handling land surface heterogeneities as well.

Acknowledgements. The authors gratefully acknowledge the fruitful discussions of this work with Randal Koster, Sharon Nebuda and Darryn Waugh. Their support and many constructive criticisms were invaluable. Discussions with Max Suarez and Mark Helfand were helpful in the development of the extended mosaic technique. D. Waugh's input during the preparation of the manuscript was extremely useful. The authors also wish to acknowledge the extremely thorough reading and many helpful comments of an anonymous reviewer that prompted an important clarification of the energy budget balance. The computing resources for these experiments were provided by the NASA Data Assimilation Office. One of the authors (HS) wishes to acknowledge the support of Professor Hugh Ellis, Chair of Geography and Environmental Engineering, in the pursuit of this work. AM is supported by a NASA Earth System Science graduate student fellowship.

References

Arain, M. A., E. J. Burke, Z. L. Yang and W. J. Shuttleworth, Implementing surface parameter aggregation rules in the CCM3 global climate model: regional responses at the land surface. *Hydrol. Earth Syst. Sci.* **3**, No 4, 463-476, 1999.

Arola, A. and D. P. Lettenmaier, Effects of Subgrid Spatial Heterogeneity on GCM-Scale Land Surface Energy and Moisture Fluxes. *J. Climate*, **9**, 1339-1349, 1996.

Avissar, R., A statistical-dynamical approach to parameterize subgrid-scale land-surface heterogeneity in climate models. In Wood, E.F. (ed.), *Land Surface-Atmosphere Interactions for Climate Modelling*, Kluwer Academic Publishers, Dordrecht, 155-178, 1991.

T. H. Chen, A. Henderson-Sellers, P. C. D. Milly, A. J. Pitman, A. C. M. Beljaars, J. Polcher, F. Abramopolous, A. Boone, S. Chang, F. Chen, Y. Dai, C. E. Desborough, R. E. Dickinson, L. Dümenil, M. Ek, J. R. Garratt, N. Gedney, Y. M. Gusez, J. Kim, R. Koster, E. A. Kowalczyk, K. Laval, J. Lean, D. Lettenmaier, X. Liang, J.-F. Mahfouf, H.-T. Mengelkamp, K. Mitchell, O. N. Nasonova, J. Noilhan, A. Robock, C. Rosenzweig, J. Shaake, C. A. Schlosser, J.-P. Schulz, Y. Shao, A. B. Shmakin, D. L. Verseghy, P. Wetzel, E. F. Wood, Y. Xue, Z.-L. Yang and Q. Zeng, Cabauw Experimental Results from the Project for Intercomparison of Land-Surface Parameterization Schemes. *J. Climate*, **10**, 1194-1215, 1997.

Cooper, H. J., E. A. Smith, J. Gu and S. Shewchuk, Modeling the Impact of Averaging on Aggregation of Surface Fluxes. *J. Geophys. Res.*, **102**, 29235-29253, 1997.

DeFries, R. S. and J. R. G. Townshend, NDVI-derived land cover classification at global scales. *Intl J. of Remote Sensing*, **15**, 3567-3586, Special Issue on Global Data Sets, 1994.

C. E. Desborough and A. J. Pitman, The BASE Land Surface Model. *Global and Planetary Change*, **19**, 3-18, 1998.

Dickinson, R., A. Henderson-Sellers, P. Kennedy and M. Wilson, Biosphere-Atmosphere Transfer Scheme (BATS) for NCAR Community Climate Model. *Tech. Note TN 275+STR*, 69pp., Nat. Cent. for Atmos. Res., Boulder, Colo, 1986.

Dirmeyer P. A., A. J. Dolman and N. Sato, The pilot phase of the Global Soil Wetness Project. *Bull. Amer. Meteorol. Soc.*, **80**(5), 851-878, 1999

Dorman, J. L., and P. J. Sellers, A global climatology of albedo, roughness length and stomatal resistance for atmospheric general circulation models as represented by the Simple Biosphere model (SiB). *J. Appl. Meteor.*, **28**, 833-855, 1989.

N. I. Ducoudre, K. Laval and A. Perrier, SECHIBA, a New Set of Parameterizations of the Hydrologic Exchanges at the Land-Atmosphere Interface within the LMD Atmospheric General Circulation Model. *J. Climate* **6**, 248-273, 1993.

Entekhabi, D. and P. S. Eagleson, Land surface hydrology parameterization for atmospheric general circulation models including subgird scale spatial variability. *J. Climate* **2**, 816-831, 1989.

Gates, W. L. (ed.), The Proceedings of the First International AMIP Scientific Conference. *WCRP-92, WMO/TD-No. 732*, World Climate Research Programme, World Meteorological Organization, Geneva, 532pp, 1995.

Giorgi, F. and R. Avissar, Representation of Heterogeneity Effects in Earth System Modeling: Experience from Land Surface Modeling. *Rev. Geophys.*, **35**, No 4, 413-438, 1997.

Helfand, H. M., M. and S. D. Schubert, Climatology of the Simulated Great Plains Low-Level Jet and Its contribution to the Continental Moisture Budget of the United States. *J. Climate*, **8**, 784-806, 1995.

Helfand, H. M., and J. C. Labraga, Design of a non-singular level 2.5 second-order closure model for the prediction of atmospheric turbulence. *J. Atmos. Sci.*, **45**, 113-132, 1988.

Henderson-Sellers, A., A.J. Pitman, P.K. Love, P. Irannejad, and T.H. Chen, The Project for Intercomparison of Land-Surface Parameterization Schemes (PILPS): Phases 2 and 3, *Bull. Amer. Meteorol. Soc.*, **76**, 489-503, 1995.

Henderson-Sellers, A. and A. J. Pitman, Land-Surface Schemes for Future Climate Models: Specification, Aggregation, and Heterogeneity. *J. Geophys. Res.*, **97**, 2687-2696, 1992.

Houser, P. R., R. Yang, J. Joiner, A. DaSilva and S. Cohn, Land Surface GEOS Modeling and Data Assimilation Strategy, DAO Office Note, Office Note Series on Global Modeling and Data Assimilation, Goddard Space Flight Center, Greenbelt, MD 20771, 21pp, 1997.

Klink, K., Surface Aggregation and Subgrid-Scale Climate. *Int. J. Climatol.*, **15**, 1219-1240, 1995.

Koeppe, C. E. and G. C. DeLong, *Weather and Climate*, McGraw Hill Book Company, U.S.A., 341 pp., 1958.

Koster, R. D., and M. J. Suarez, Modeling the Land Surface Boundary in Climate Models as a Composite of Independant Vegetation Stands. *J. Geophys. Res.*, **97**, 2697-2715, 1992a.

Koster, R. D., and M. J. Suarez, A Comparitive Analysis of Two Land Surface Heterogeneity Representations. *J. Climate*, **5**, 1379-1390, 1992b.

Koster, R. D., and M. J. Suarez, Energy and Water Balance Calculations in the MOSAIC LSM. NASA Technical Memorandum 104606 Volume 9, Technical Report Series on modeling and Data Assimilation, Max J. Suarez, ed., Goddard Space Flight Center, Greenbelt, MD 20771, 76 pp, 1992c.

Leetma, A. and R. W. Higgins, Reanalysis and the Development of Climate Forecast Systems. Proceedings of the Second International Conference on Reanalysis, Reading, U.K. 23-27 August, 1999.

Mahfouf, J.-F., A. O. Manzi, J. Noilhan, H. Giordani and M. Deque, The Land Surface Scheme ISBA within the Meteo-France Climate Model ARPEGE. Part I. Implementation and Preliminary Results. *J. Clim.*, **8**, 2039-2057, 1995.

Milly, P. and K. A. Dunne, Sensitivity of Global Water Cycle to the Water Holding Capacity of Land. *J. Climate*, **7**, 506-526, 1994.

Mitchell, K., P. Houser, E. Wood, J. Schaake, D. Tarpley, D. Lettenmaier, W. Higgins, C. Marshall, D. Lohmann, M. Ek, B. Cosgrove, J. Entin, Q. Duan, R. Pinker, A. Robock, F. Habets and K. Vinnikov, The GCIP Land Data Assimilation System (LDAS) Project – Now Underway. *GEWEX News* November, 1999.

Mölders, N, A. Raabe and G. Tetzlaff, A Comparison of Two Strategies on Land Surface Heterogeneity Used in a Mesoscale β Meteorological Model. *Tellus*, **48A**, 733-749, 1996.

Molod, A., The Land Surface Component in GEOS: Model Formulation. DAO Office Note 1999-03, Office Note Series on Global Modeling and Data Assimilation, Goddard Space Flight Center, Greenbelt, MD 20771, 21pp, 1999.

Molod, A., Helfand, H. M., and L. L. Takacs, The Climatology of Parameterized Physical Processes in the GEOS-1 GCM and their Impact on the GEOS-1 Data Assimilation System. *J. Climate*, **9**, 764-785, 1996.

Pan, H.-L. and L. Mahrt, Interaction Between Soil Hydrology and Boundary Layer Development. *Bound. Lay. Meteorol.*, **38**, 185-202, 1987.

Polcher, J., K. Laval, L. Dümenil, J. Lean and P. R. Rowntree, Comparing Three Land Surface Schemes Used in General Circulation Models. *J. Hydrol.*, **180**, 373-394, 1996.

Polcher, J., Sensitivity of Tropical Convection to Land Surface Processes. *J. Atmos. Sci.*, **52**, 3143-3161, 1995.

Rosenzweig, C. and F. Abramopoulos, Land-Surface Model Development for the GISS GCM. *J. Climate*, **10**, 2040-2054, 1997.

Schubert, S. D., C.-K. Park, C.-Y. Wu, R. W. Higgins, Y. Kondratyeva, A. Molod, L. L. Takacs, M. Seablom and R. Rood, A Multi-Year Simulation with the GEOS-1 System: Overview and Results. NASA Tech. Memo 104606 Volume 6, NASA/Goddard Space Flight Center, Greenbelt, MD, 183 pp, 1995.

Schubert, S. D., J. Pfaendtner and R. Rood, An assimilated data set for Earth Science applications. *Bull. Amer. Meteor. Soc.*, **74**, 2331-2342, 1993.

Sellers, P. J., Y. Mintz, Y. C. Sud and A. Dalcher, A Simple Biosphere Model (SiB) for Use within General Circulation Models. *J. Atmos. Sci.*, **43**, 505-531, 1986.

van den Hurk, B. J. J. M. and A. C. M. Beljaars, Impact of Some Simplifying Assumptions in the New ECMWF Surface Scheme. *J. Applied Meteorol.*, **35**, 1333-1343, 1996.

Verseghy, D. L., N. A. McFarlane and M. Lazare, CLASS - A Canadian Land Surface Scheme for GCMs, II. Vegetation Model and Coupled Runs. *Int. J. Climatol.*, **13**, 347-370, 1993.

Viterbo, P. and A. C. M. Beljaars, An Improved Land Surface Parameterization Scheme in the ECMWF Model and its Validation. *J. Clim.*, **8**, 2716-2748, 1995.

Wu, M.-L. C., S. Schubert, and N. E. Huang, The development of the South Asian Summer Monsoon and the Intraseasonal Oscillation. *J. Climate*, **12**, 2054-2075, 1999.

Xue, Y., P. J. Sellers, J. L. Kinter III and J. Shukla, A Simplified Biosphere Model for Global Climate Studies. *J. Clim.*, **4**, 345-364, 1991.

List of Captions

Definition of Geographical Regions

Region	Longitude	Latitude	VI $\times 100$
Alaska	160W to 140W	60N to 72N	17
Amazon	70W to 50W	10S to 2N	0
Australia	120E to 140E	30S to 18S	4
Boreal Forest	120W to 100W	50N to 62N	13
Central Plains	105W to 85W	34N to 46N	13
Central S. Amer.	65W to 45W	22S to 10S	15
China	100E to 120E	30N to 42N	12
Eurasia	20E to 40E	40N to 52N	18
Newfoundland	80W to 60W	48N to 60N	11
Russia	80E to 100E	60N to 72N	25
Sahara	5W to 15E	18N to 30N	2
Siberia	115E to 135E	54N to 66N	35
Southeast US	95W to 80W	30N to 36N	22
Southern Africa	15E to 35E	30S to 18S	10
South S. Amer.	70W to 60W	42S to 25S	13

Table 1: Definitions and locations of the fifteen climatic regions

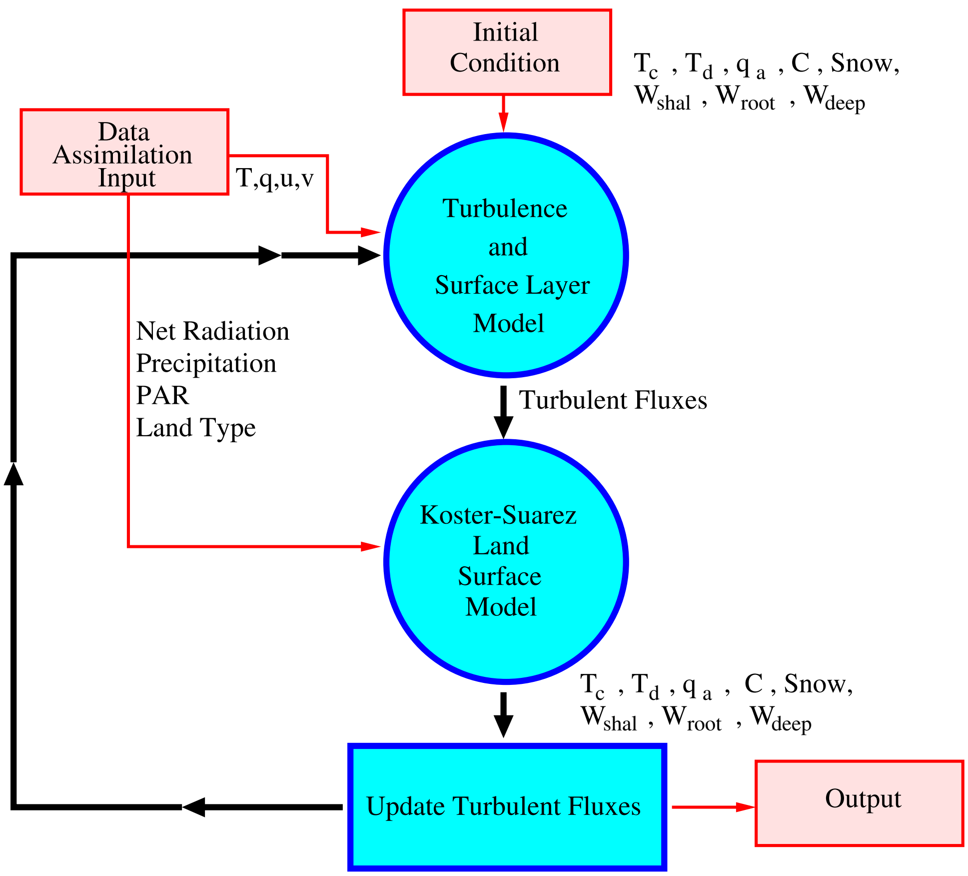

Figure 1: A Schematic of the OLGA experimental framework.

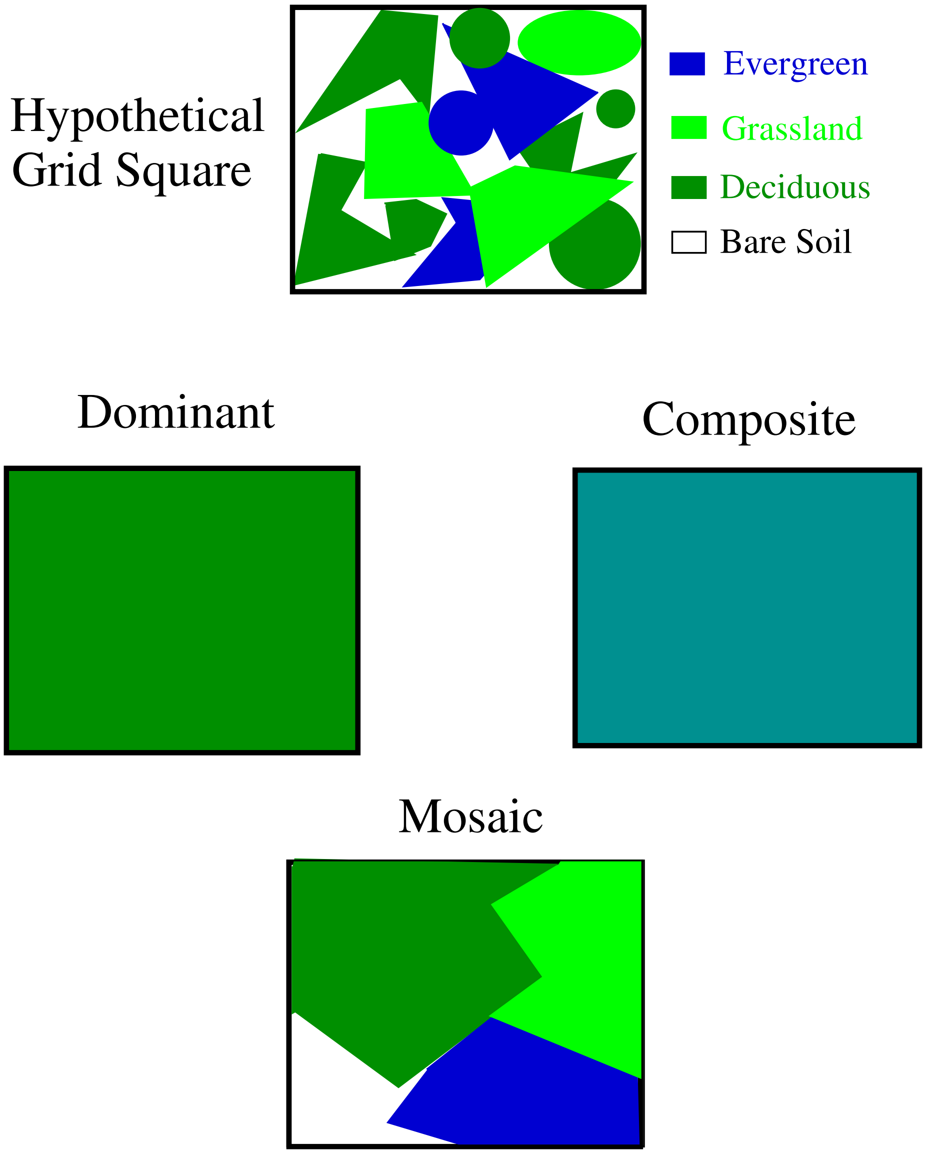

Figure 2: Schematic of Different Aggregation Techniques.

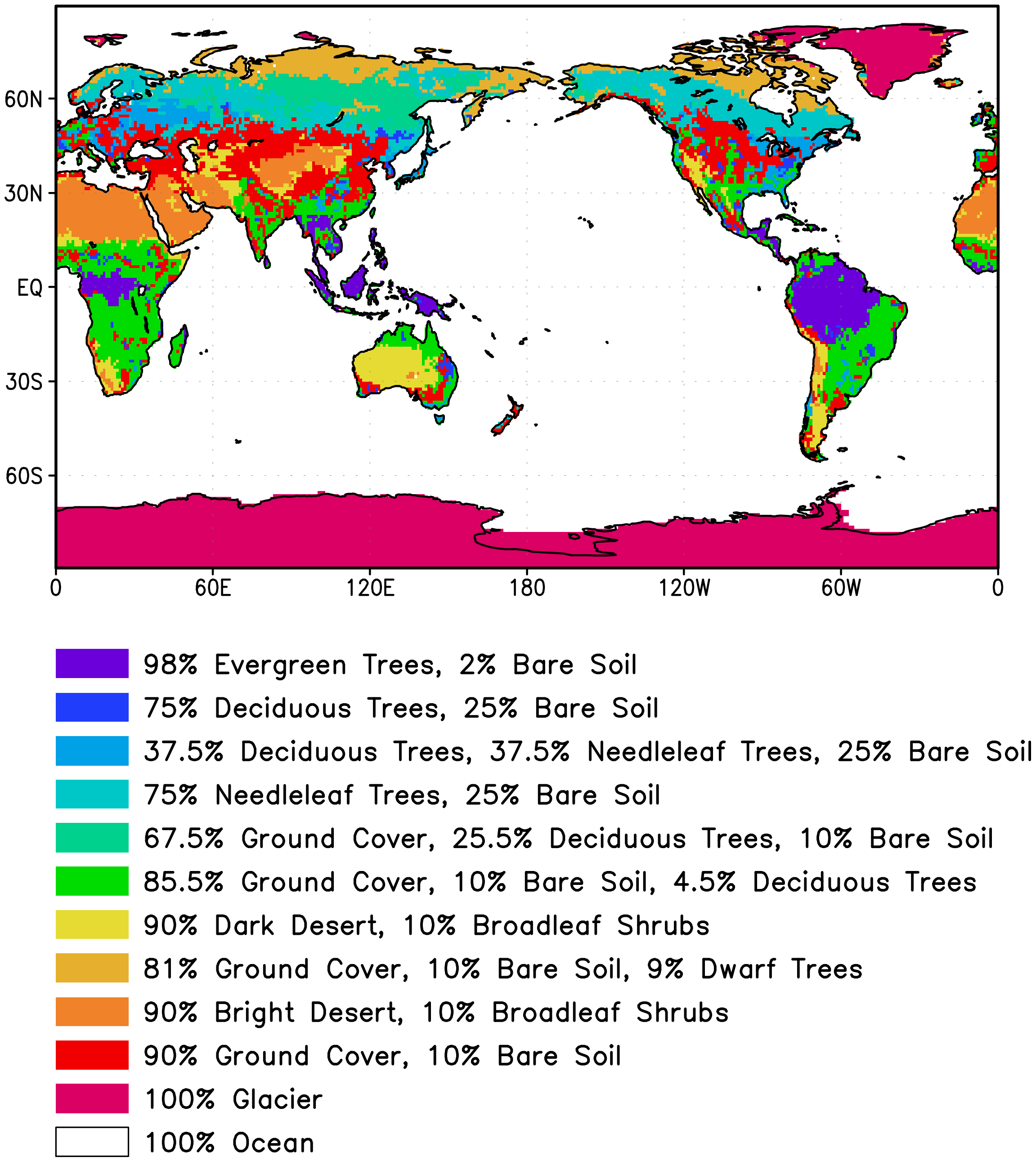

Figure 3: GEOS-Terra GCM surface type combinations.

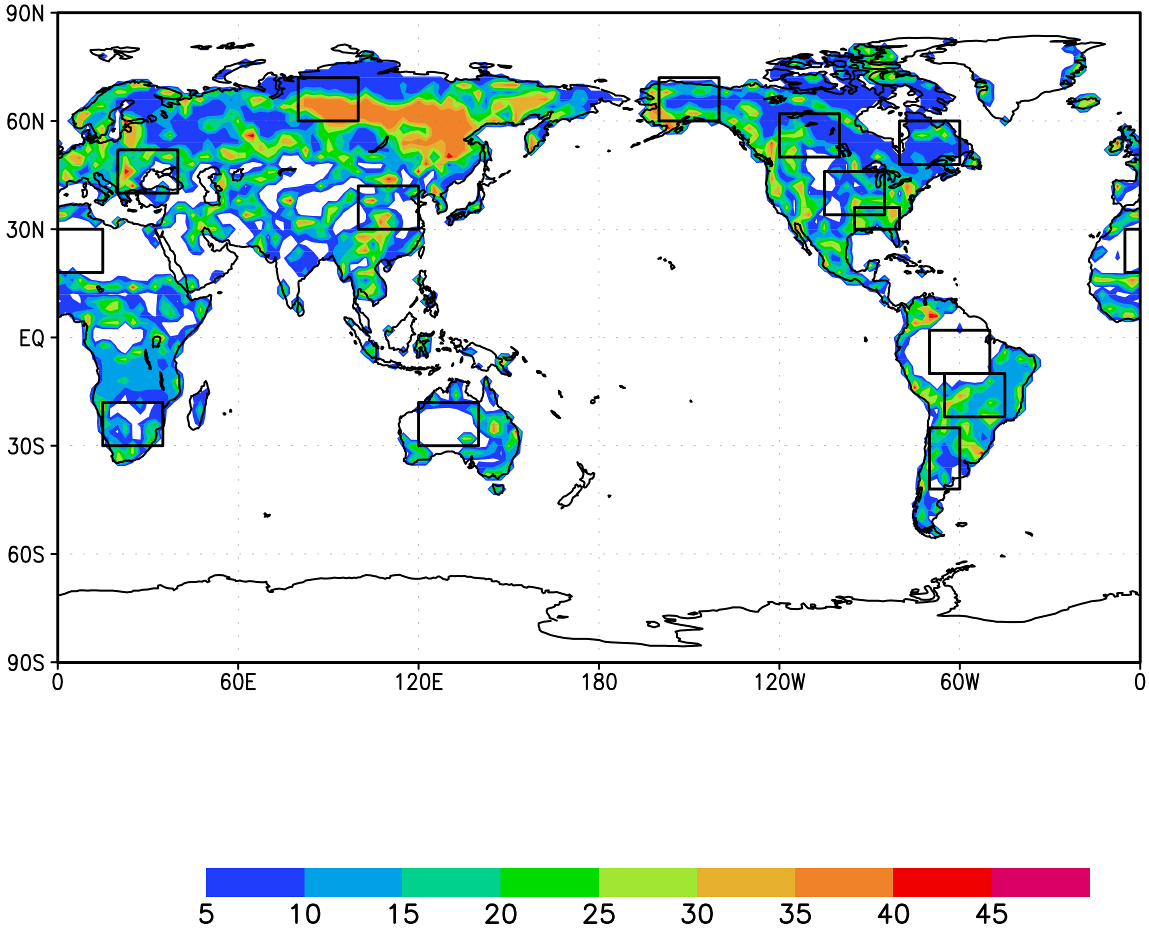

Figure 4: Variability Index ($\times 100$) and the fifteen regions defined in this study

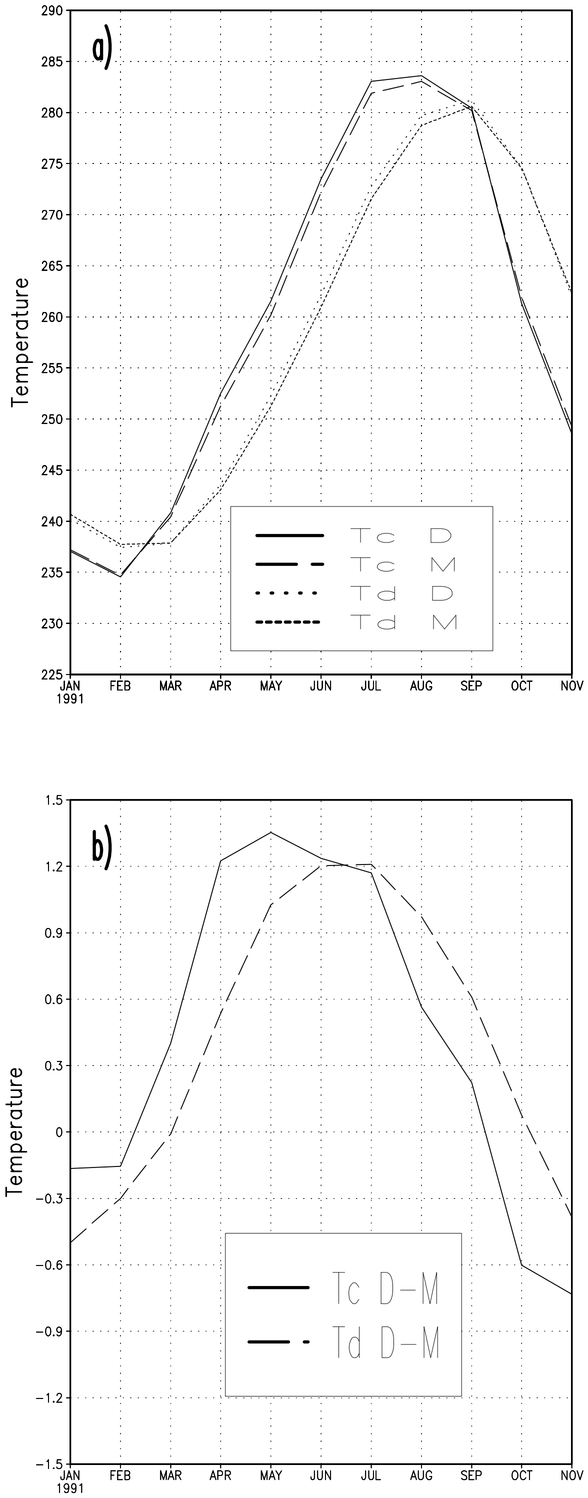

Figure 5: Russia region results, which are a prototype for NHL. a) Canopy temperature and deep soil temperature, in K, b) canopy temperature and deep soil temperature D-M differences, c) surface and root zone soil moisture, in fraction of field capacity (wilting point near 0.18), and d) surface and root zone soil moisture D-M differences.

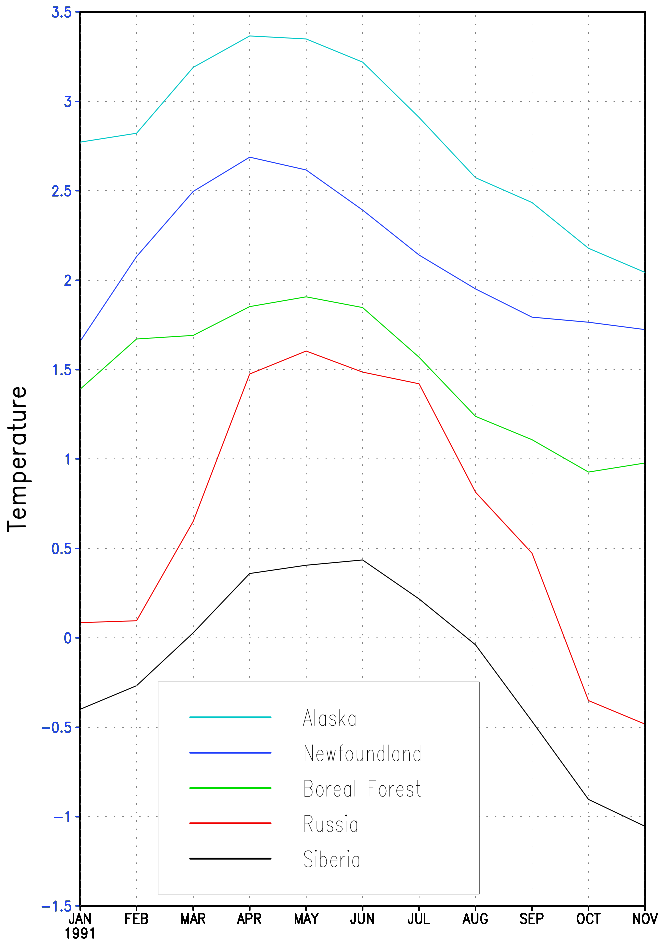

Figure 6: Canopy temperature D-M differences for Northern High Latitude (NHL) regions in K. Each curve is displaced vertically as follows: Siberia is not displaced, Russia by $0.25K$, Boreal Forest by $1.75K$, Newfoundland by $2.25K$ and Alaska by $2.75K$

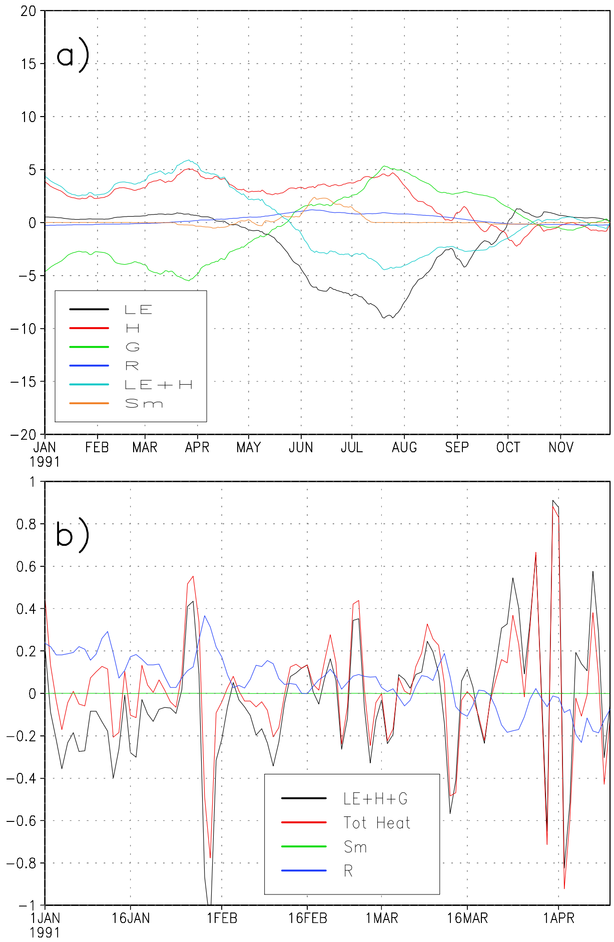

Figure 7: a) 30-day running mean D-M differences in the various terms in the surface energy budget in W/m^2 for the Russia region, and b) residual budget terms measured against the total temperature tendency in units of W/m^2. Curves plotted on an expanded scale relative to a). The notation 'Tot Heat' in the legend is used for the term $C_h \frac{\delta T_c}{\delta t}$.

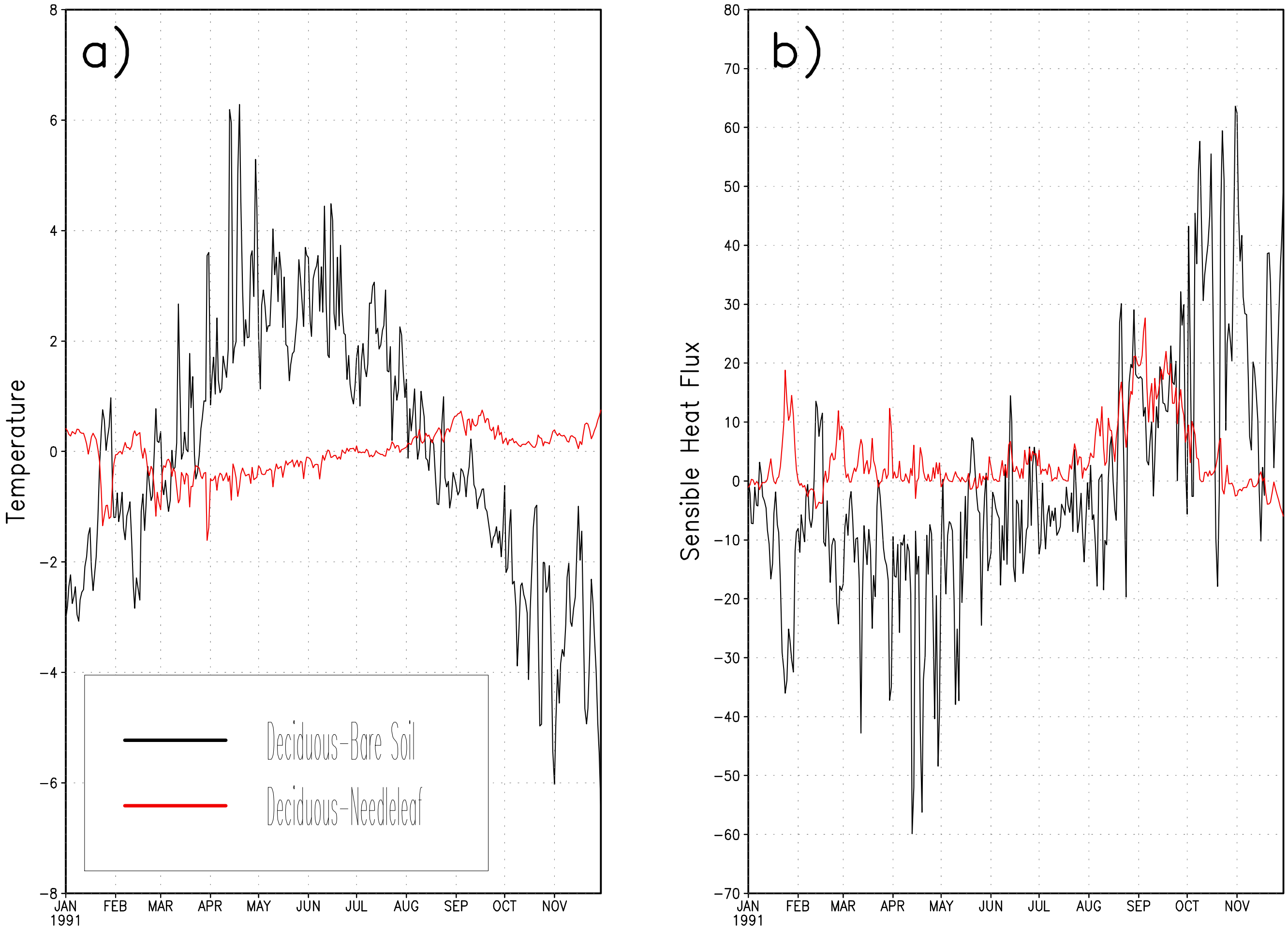

Figure 8: Daily time series for the subregion of Russia defined in the text of a) canopy temperature differences between tiles in K, and b) sensible heat flux differences between tiles in W/m^2. The black lines are the differences between the deciduous trees tile and the bare soil tile, and the red lines are the differences between the deciduous trees tile and the needleleaf trees tile.

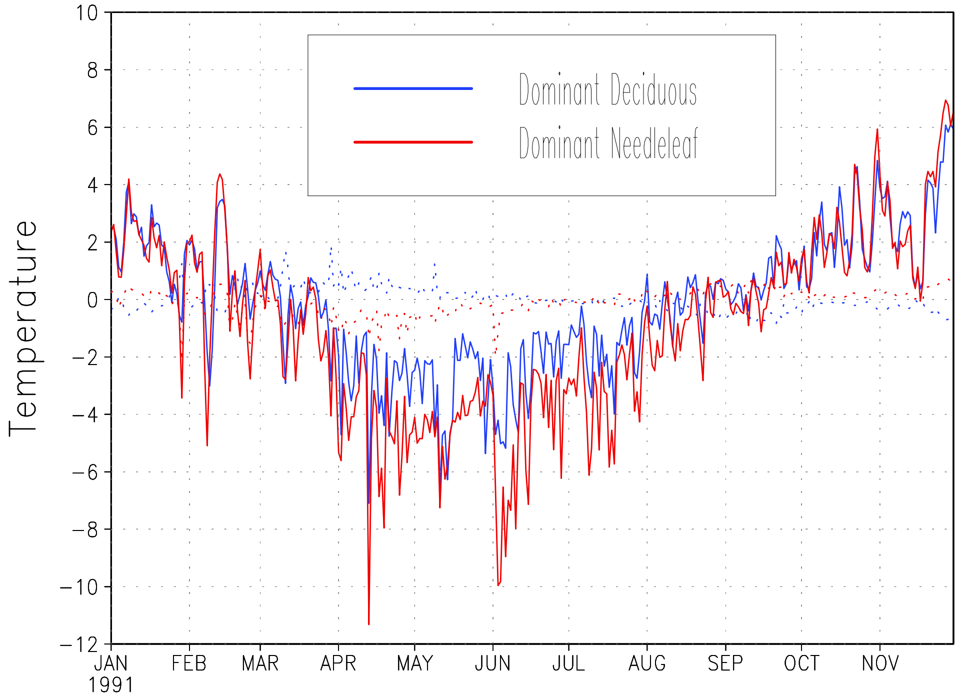

Figure 9: Daily time series of canopy temperature differences between tiles in K for two different grid boxes. The two solid lines (one red and one blue) are the differences between the bare soil tile and the dominant tile in each grid box, and the two dotted lines are the differences between the other vegetated tile and the dominant tile in each grid box.

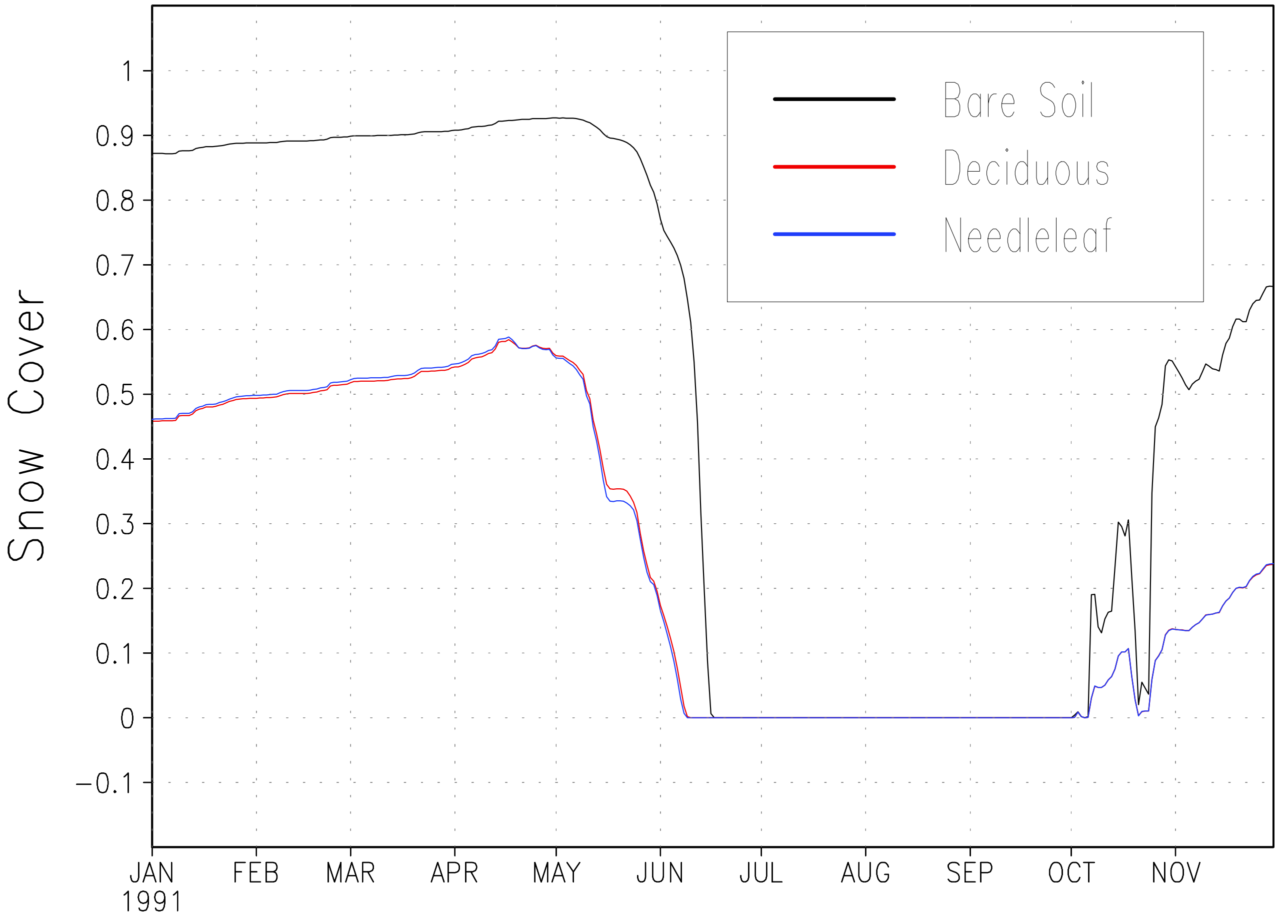

Figure 10: Daily time series of the snow fraction for different tiles in the grid boxes of the subregion of Russia defined in the text and used in figure 8.

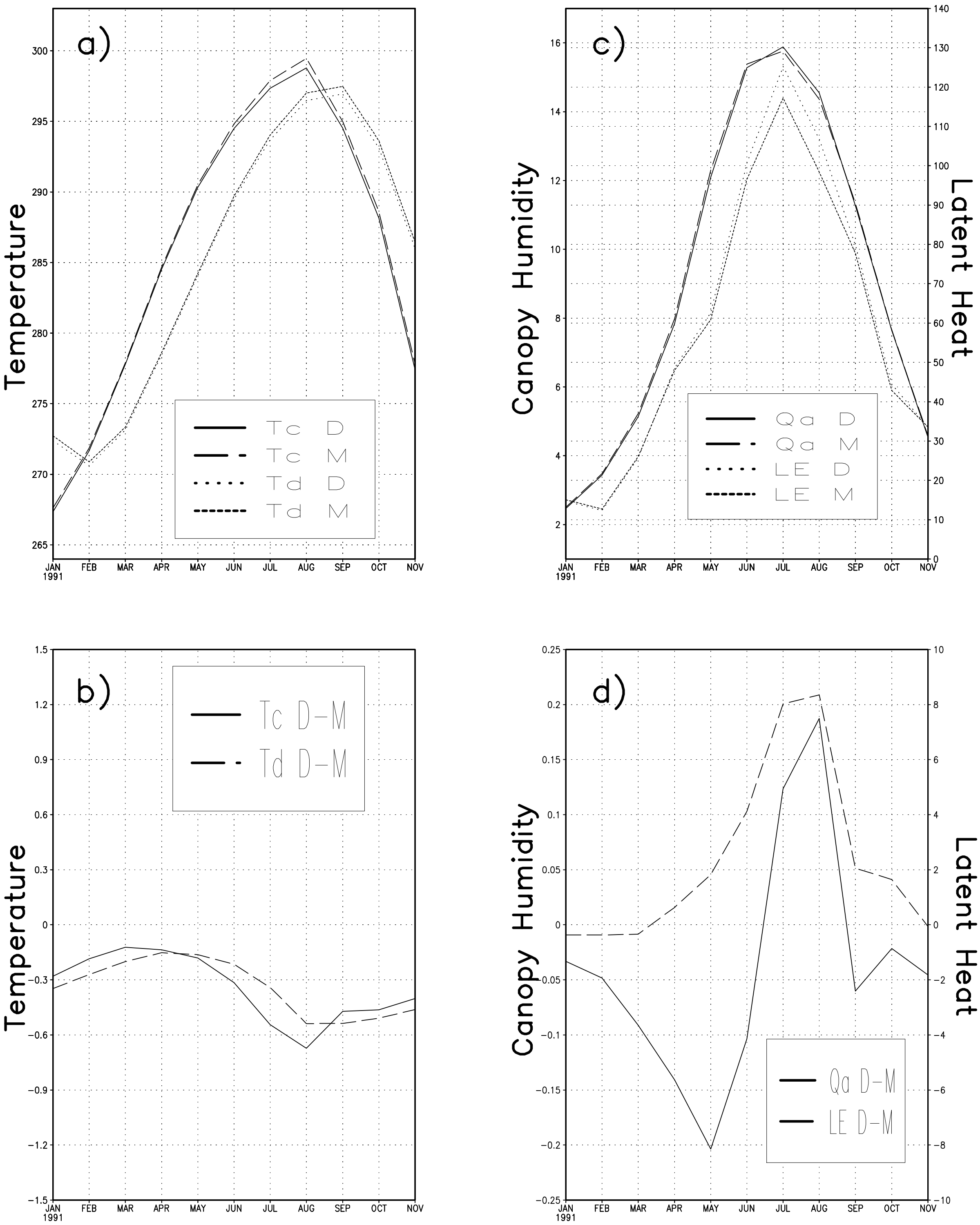

Figure 11: Central Plains region results, which are a prototype for NML. a) Canopy temperature and deep soil temperature, in K, b) canopy temperature and deep soil temperature D-M differences, c) canopy humidity, in g/kg on the left vertical scale, and latent heat flux, in W/m^2 on the right vertical scale, and d) D-M differences in canopy humidity (left scale) and latent heat flux (right scale).

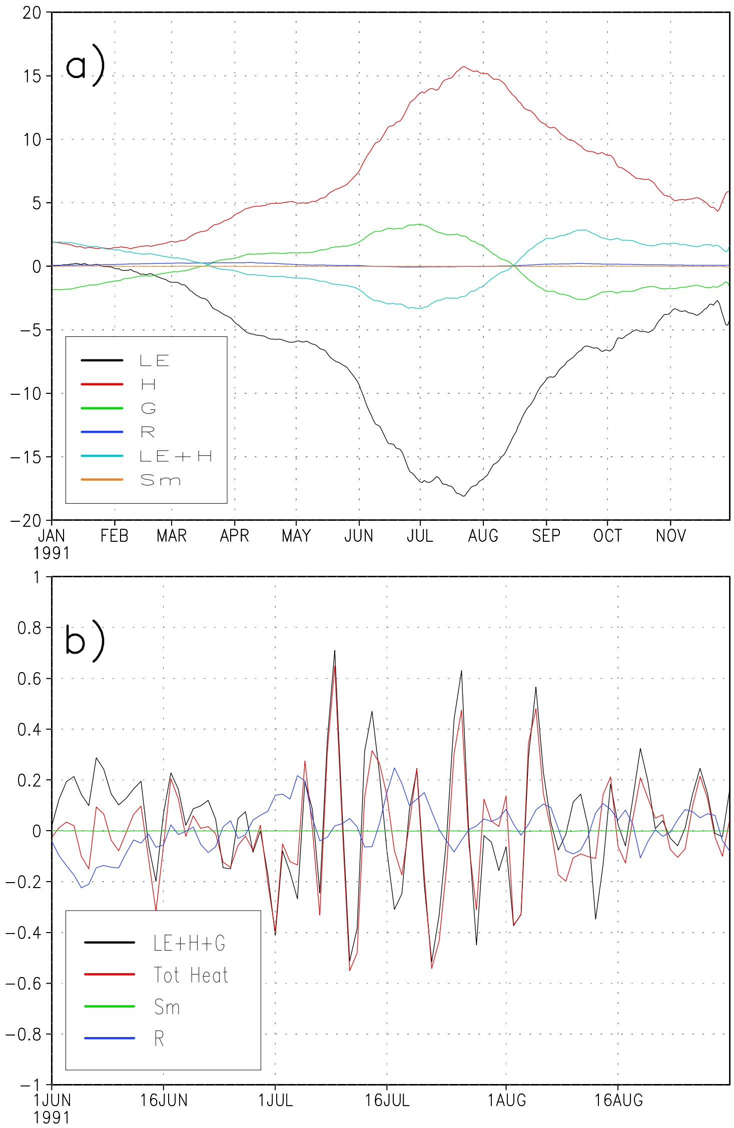

Figure 12: a) 30-day running mean D-M differences in the various terms in the surface energy budget in W/m^2 for the Central Plains region, and b) residual budget terms measured against the total temperature tendency in units of W/m^2. Curves plotted on an expanded scale relative to a). The notation 'Tot Heat' in the legend is used for the term $C_h \frac{\delta T_c}{\delta t}$.

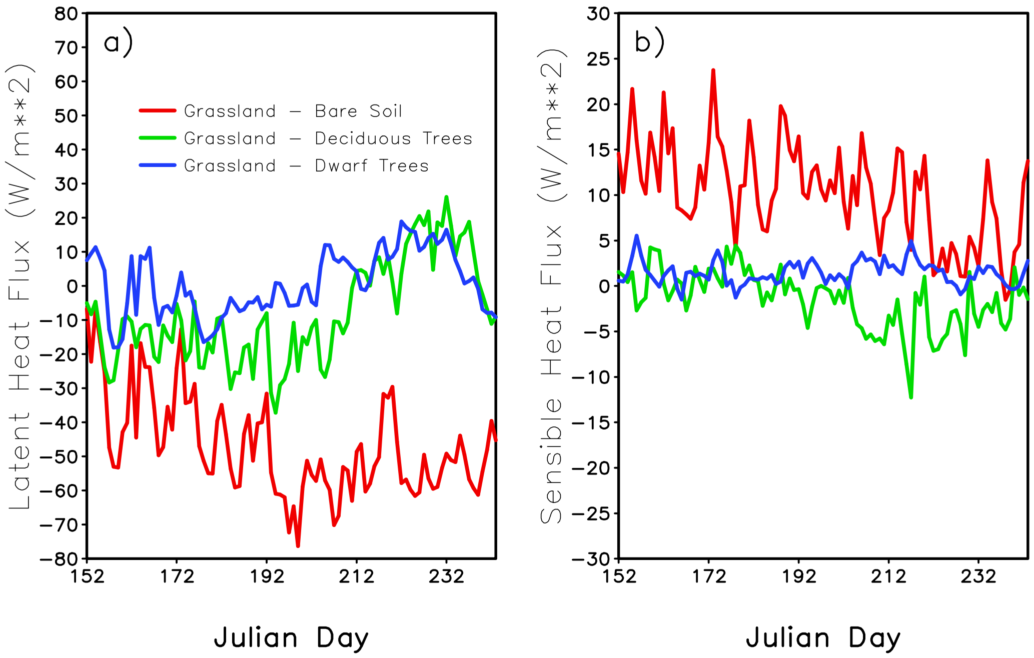

Figure 13: Daily time series for the Central Plains region of a) latent heat flux differences between tiles in W/m^2, and b) sensible heat flux differences between tiles in W/m^2. The red lines are the differences between the grassland tile and the bare soil tile, the green lines are the differences between the grassland and deciduous trees tiles and the blue lines are the differences between the grassland tile and the dwarf trees tile.

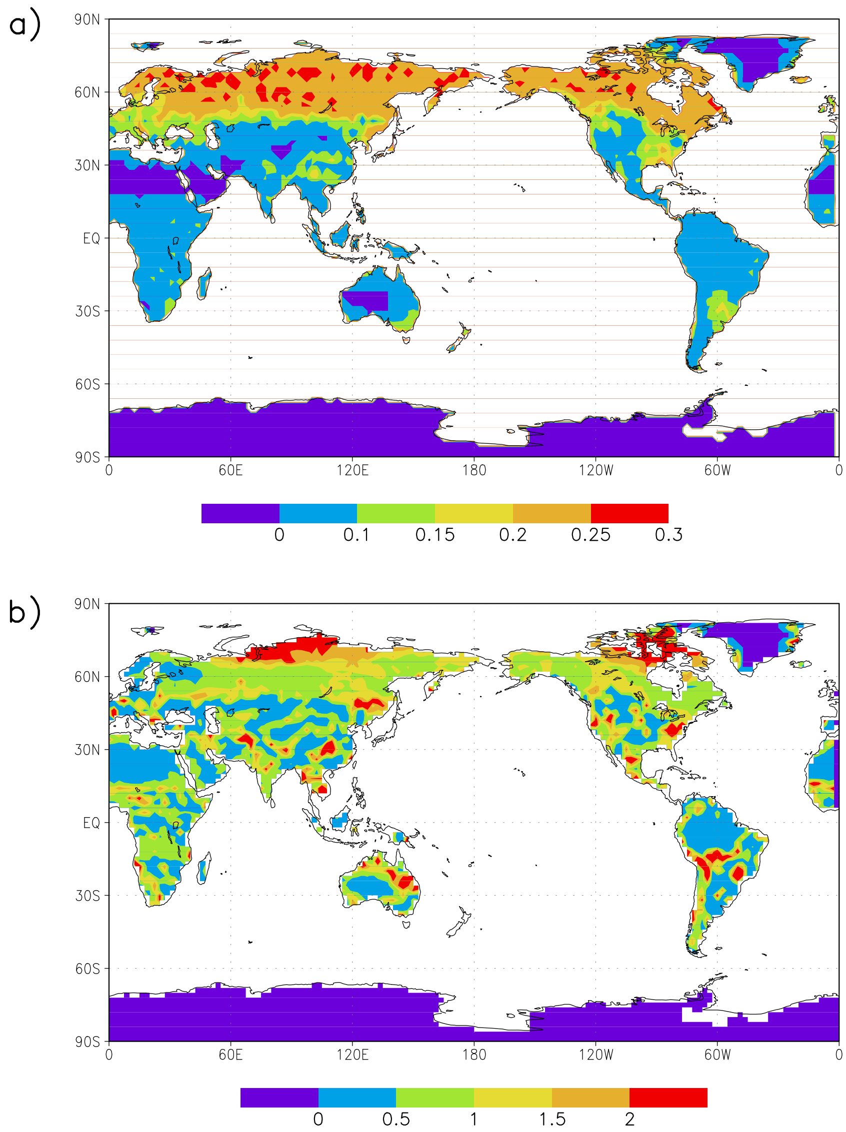

Figure 14: a) Off-dominant bare soil fraction, b) absolute value of the maximum D-M canopy temperature difference during the year in K.